Synthesis, Characterization, Optical, and Dielectric Properties of Polyvinyl Chloride/Cadmium Oxide Nanocomposite Films

A.M. El Sayed,[1] S. El-Sayed,[1,2] W.M. Morsi,[3] S. Mahrous,[1] A. Hassen[1,2]
[1]*Department of Physics, Faculty of Science, Fayoum University, Fayoum 63514, Egypt*

[2]*Department of Physics, Faculty of Science and Education, Al Khurma Branch, Taif University, Saudi Arabia*

[3]*Building Physics Institute, Housing and Building National Research Center, HBRC, Dokki, Giza 11511, Egypt*

Nano-sized cadmium oxide (CdO) was synthesized using a sol–gel method and mixed with poly(vinyl chloride) (PVC). X-ray diffraction and high-resolution transmission electron microscopy measurements indicated that the average particle size of the CdO is about 70.18 nm. Scanning electron microscopy images revealed a good dispersion of CdO nanoparticles on the surface of the PVC films. The optical energy band gap (E_g) showed a decrease from 5.08 to 4.88 eV with increasing the CdO content. The refractive index dispersion of the nanocomposite films was found to obey the single oscillator model. The dispersion parameters were changed by CdO incorporation. According to the frequency and temperature dependence of the dielectric constant (ε'), the observed α_a-relaxation peaks were assigned to the micro-Brownian motion of the polymer main chains. The influence of CdO nanoparticles content on the ac conductivity and the activation energy of PVC nanocomposite films were discussed. It was found that both dielectric and optical properties were reinforced by the adding of CdO nanoparticles to the PVC matrix. Finally, the results of the present system are compared with those of similar materials. POLYM. COMPOS., 35:1842–1851, 2014. © 2014 Society of Plastics Engineers

INTRODUCTION

In the recent years, nanocomposite materials have received great interest for both industrial and academic applications [1, 2]. This is due to the fact that a small amount of the nano-additives could improve the overall performances of the polymeric materials. This is owing to the small size, large specific area, quantum confinement effects, and the strong interfacial interaction of the nanomaterials [3]. Poly(vinyl chloride) (PVC) is one of the most massive produced and consumed polymers over the world [4]. It has low thermal conductivity of 0.014 W/(m K), high-flame retardancy, and high chemical resistance and, hence, it has been extensively used as a thermoplastic material [5–10]. PVC/graphite nanocomposites could be used for attenuation and electromagnetic interference shielding [11, 12]. PVC/($Cd_{0.5}Zn_{0.5}O$) nanocomposites were reported to have high transparency, high UV-shielding efficiency, and improved thermal stability [13]. PVC/ZnO nanocomposites showed higher glass transition temperature (T_g), specific heat, and thermal stability relative to those of pure PVC [14]. It was also reported that PVC/ZnO-polyaniline hybrid nanocomposites have a dramatically increased corrosion protection effect on iron [15]. In fact, there are many reports on different PVC-based nanocomposites. These include the addition of Al_2O_3, SiO_2, and TiO_2 nanoparticles to PVC [6, 9, 10], nano-TiO_2@Ag [7], reduced graphite nanosheet [8], graphene nanosheet [16], $CaCO_3$ nanoparticles [17], multiwall carbon nanotubes [18]. These studies were focused mainly on the electrical, mechanical, chemical, and thermal properties of PVC nanocomposites and revealed that the properties of PVC could be significantly improved and its industrial applications can be broadened.

Cadmium oxide (CdO) is one of the promising II–VI compounds. CdO powders and films have n-type semiconducting properties, electrical resistivity in the order of 10^{-2}–10^{-4} Ω cm [19, 20] and mobility as high as $\mu = 146$ cm^{2}V^{-1} s^{-1} with $N = 1.5 \times 10^{20}$ cm^{-3} [21, 22]. In addition, CdO has a high optical transmittance in the visible region of the solar spectrum along with a refractive index of 2.49 [23, 24]. Depending on the deviation

Correspondence to: A.M. El Sayed (e-mail: ams06@fayoum.edu.eg and ad_286@yahoo.com)
DOI 10.1002/pc.22839
Published online in Wiley Online Library (wileyonlinelibrary.com).

from ideal CdO stoichiometry (e.g., due to cadmium interstitials $Cd_{(1+X)}O$ or oxygen vacancies $CdO_{(1-X)}$), its direct band gap varied from 2.2 to 2.5 eV and its indirect band gap varied from 1.36 to 1.98 eV [20, 25, 26]. Based on these properties, CdO has been used for applications such as in catalysts [26], sensors [27], and in some optoelectronic devices [24, 28]. CdO nanoparticles were prepared via different techniques; for example, solid-state reaction [19], mechanochemical method [26], and co-precipitation method [29]. Also, a green biosynthesis of CdO nanoparticles of 35 nm in size using Achillea Wilhelmsii plant was reported [30]. With this background of multifunctionality CdO, it is thought worthwhile to use the nano-sized CdO as inorganic fillers to improve the optical and dielectric properties of PVC.

Because of their excellent control of the stoichiometry, relative simplicity, and the general advantage of large area deposition, sol–gel technique, and solution casting method were chosen for the preparation of CdO nanoparticles and PVC/CdO nanocomposite films. There are few reports on the effect of adding CdO on the conductivity and dielectric relaxation of polyaniline [31, 32]. In the present work, the influences of CdO nanoparticles on the optical as well as the dielectric properties of PVC are given.

EXPERIMENTAL

Materials Preparation

CdO nanoparticles were synthesized by using a sol-gel process. First, 0.7 M solution was prepared by dissolving 16.54 g of a high-purity cadmium nitrate [$Cd(NO_3)_2$, $M_W = 236.42$, Nova Oleochem Limited] and 8.825 g of oxalic acid ($C_2H_2O_4$) in 100 ml double distilled (*DD*) water with a magnetic stirring for 2 h. The obtained sol was held in an oven at 100°C for 8 h, then cooled to 70°C and stirred to obtain the gel. This gel was aged for 18 h, then it was calcined at 400°C for 3 h to obtain CdO nanoparticles. The synthesized nanoparticles were added in different x (wt%; 0.0, 0.3, 0.7, 1.0, and 1.4) to PVC according to:

$$x(\text{wt}\%) = \frac{w_f}{(w_p + w_f)} \times 100 \quad (1)$$

where w_f and w_p represent the weights of CdO and PVC, respectively. The nanocomposite films were prepared as follows: 2.0 g PVC [Polymer Laboratories (Essex, UK)] dissolved in 70 ml Tetrahydrofuran [THF, Aldrich, Germany] with stirring for 1 h at room temperature (RT) till the complete dissolution of the polymer. The required mass of the prepared CdO powder was added to the solution under vigorous stirring at RT to prevent the agglomeration of the nanoparticles. The aqueous solutions of the mixtures were then casted into Petri dishes placed on a leveled plate and kept to dry in air at RT for 24 h. Finally, the films were peeled off from the Petri dishes and care was taken to obtain homogenous samples with the same thickness.

Characterization Techniques

The obtained CdO powder and the films of pure PVC and PVC loaded with CdO nanoparticles were characterized. X-ray diffraction (XRD) of CdO particles, PVC, and CdO-doped PVC films were performed using a PANalytical's X'Pert PRO. High-resolution transmission electron microscopy (HR-TEM; JEM 2100, Jeol, Japan) was used to test the crystalline size of the as-synthesized CdO particles. Scanning electron microscopy (SEM; Inspect S, FEI, Holland) images were taken for pure PVC and the nanocomposite films. The film thickness was evaluated using a digital micrometer with accuracy ± 0.001 mm. Optical characterization was carried out at RT using a Shimadzu UV-3600 UV–vis-NIR spectrophotometer in the wavelength range 230–800 nm with an accuracy of ± 0.2 nm. The dielectric measurements were performed in the temperature and frequency ranges of 303–468 K and 50 kHz–3 MHz, respectively, by using a Hioki (Ueda, Nagano, Japan) model 3532 High Tester LCR, with capacitance measurement accuracy on the order of 0.0001 pF. The temperature was measured with a T-type thermocouple having an accuracy of ± 1°C. The dielectric constant ε' of each sample was calculated using the relation:

$$\varepsilon' = dC/\varepsilon_o A \quad (2)$$

where C is the capacitance, d is the thickness of the sample, ε_o is the permittivity of free space, and A is the cross-sectional area of the sample.

RESULTS AND DISCUSSION

Structural Properties

X-ray Diffraction. XRD pattern of the sol–gel synthesized CdO nanoparticles is shown in Fig. 1(a). All of the diffraction peaks can be indexed to the cubic phase of CdO with a lattice parameter $a = 4.69483$ Å and Fm3m space group. The peaks at 2θ values of 33.08°, 38.40°, 55.39°, 66.0°, and 69.39° are matching with the (110), (200), (220), (311), and (222) plans, respectively (Joint Committee for Powder Diffraction Studies (JCPDS) File No. 75-0592). This indicates the formation of CdO with excellent crystallinity [27]. No second phases were observed indicating a high purity of the synthesized CdO nanoparticles. The crystallite size (D) of the CdO nanoparticles was determined using the well known Scherer's formula, $D = 0.9\lambda/(B\cos\theta)$, where B is the full width at half maximum intensity (FWHM) and $\lambda = 1.54$ Å. From XRD, the crystallite size of CdO is ranged from 66.4 to 73.2 nm with an average of $D_{av} = 70.18$ nm as given in Table 1. Vidyasagar et al. [19] synthesized Cu–doped CdO plate-like particles of size 70–168 nm via a solid-state

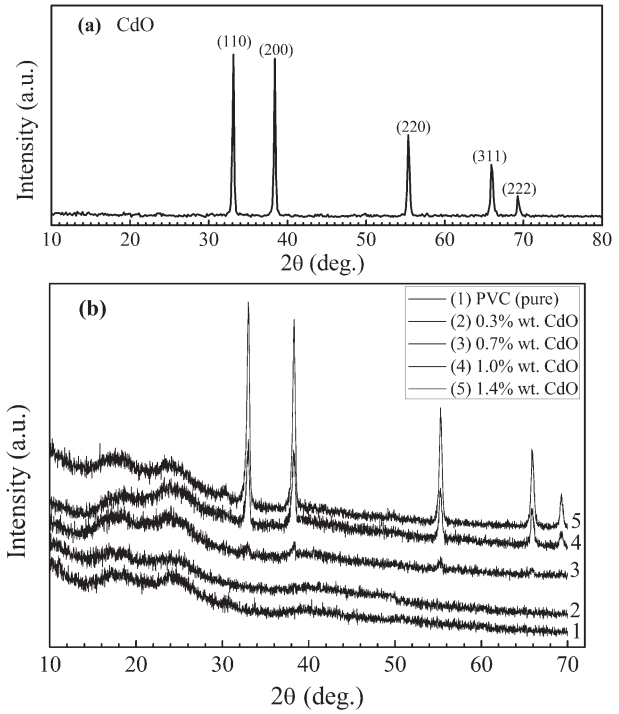

FIG. 1. XRD patters for: (a) CdO nanoparticles, and (b) pure PVC and PVC loaded with different amounts of CdO nanoparticles.

reaction. Bazargan et al. [24] prepared CdO nanofibers of diameter range 50–60 nm using the electrospinning technique. Also, Tadjarodi et al. [27] reported the synthesis of CdO nanoparticles (~41 nm) by milling the cadmium nitrate tetrahydrate and acetamide at RT followed by calcination at 450°C. Fig. 1(b) shows the XRD patterns of PVC and PVC loaded with CdO nanoparticles. For pure PVC, the broad peak, halo, in the region of 15–35°, indicates the amorphous nature of PVC [33, 34]. By comparing the XRD pattern of pure PVC with its nanocomposites, it is observed that there is a homogenous distribution of CdO in PVC and the diffraction peaks of CdO are seen clearly starting from the CdO content of 0.7 wt%. CdO retains its cubic structure even though dispersed in PVC.

Characterization. HR-TEM image of the as-prepared CdO nanoparticles was taken to determine the crystal size. It can be seen from Fig. 2(a) that CdO nanoparticles are well defined and ranged from 51.98 to 115.9 nm with average particle size ≈71.7 nm, which is in agreement with the results of XRD. It is noteworthy to mention that the average crystallite size deduced from XRD data is well consistent with that observed from HR-TEM. This indicates that our synthesis process is suitable for obtaining CdO nanoparticles. In addition, SEM was performed to examine the morphology and dispersion of CdO nanoparticles on the surface of PVC films. Fig. 2(b–f) shows SEM images for pure PVC and PVC/CdO nanocomposite films. As seen, CdO nanoparticles are well dispersed on the surface of the PVC.

TABLE 1. XRD data and particle size (D) of CdO.

Sample	2θ (°)	d-Spacing (Å)	I/I_o%	D (nm)
CdO	33.082	2.705	100	69.5
	38.40	2.342	89.9	73.2
	55.39	1.657	50.4	69.3
	66.00	1.414	35.7	66.4
	69.39	1.354	14.6	72.5
D_{av} = 70.18 nm				

Optical Properties

The study of the UV–vis absorption spectra is a direct and simple method for probing the band structure of the investigated samples. The UV–vis absorption spectra of pure PVC and PVC loaded with CdO nanoparticles are shown in Fig. 3(a). The absorbance increases with increasing the CdO content in the PVC matrix. An absorption band at ~256 nm is observed for pure PVC and assigned to π–π^* transition [35, 36]. This band is enhanced in the spectra of the PVC/CdO nanocomposite films. The significant increase in the absorbance below 256 nm is associated with the C—Cl bond [37]. Also, a small hump around 485 nm is observed specially for 1.4 wt% CdO-doped PVC film. Such a hump may be attributed to the formation of charge transfer complexes [38]. As seen in Fig. 3(b), PVC is an optically transparent polymer with transmission (T) over 90% in the visible region. Similar results were found for the other nanocomposite films, i.e., there is no evidence on nanoparticles agglomeration as seen by SEM. CdO nanoparticles inside PVC matrix may act as scattering centers, which cause the observed decrease in T% with increasing CdO content. Once again, there is a difference in the optical properties of the sample 1.4 wt% of CdO-loaded PVC and those of the other investigated nanocomposite films. This deviation in results (Fig. 3(a, b)) may be attributed to the formation of some aggregates of CdO nanoparticles within the PVC. Similar deviation was also observed for 0.75 wt% of Cr_2O_3 nanoparticles filled PVA [38] and 3 wt% of ZnO nanorodes loaded with PVA [39].

Using the observed UV–vis spectra, the direct energy band gap (E_g) was determined according to the frequency dependence of the absorption coefficient, α, (where α = absorbance /film thickness) and by using Tauc's relation [8, 34, 40, 41]:

$$\alpha h\upsilon = B(h\upsilon - E_g)^m \quad (3)$$

where $h\upsilon$ is the incident photon energy that can be approximated to $h\upsilon = 1240/\lambda$, B is a constant having values between 1×10^5 and 1×10^6 (cm eV)$^{-1}$ [42, 43], and m assumes to be 1/2, 2 for allowed direct and

DOI 10.1002/pc

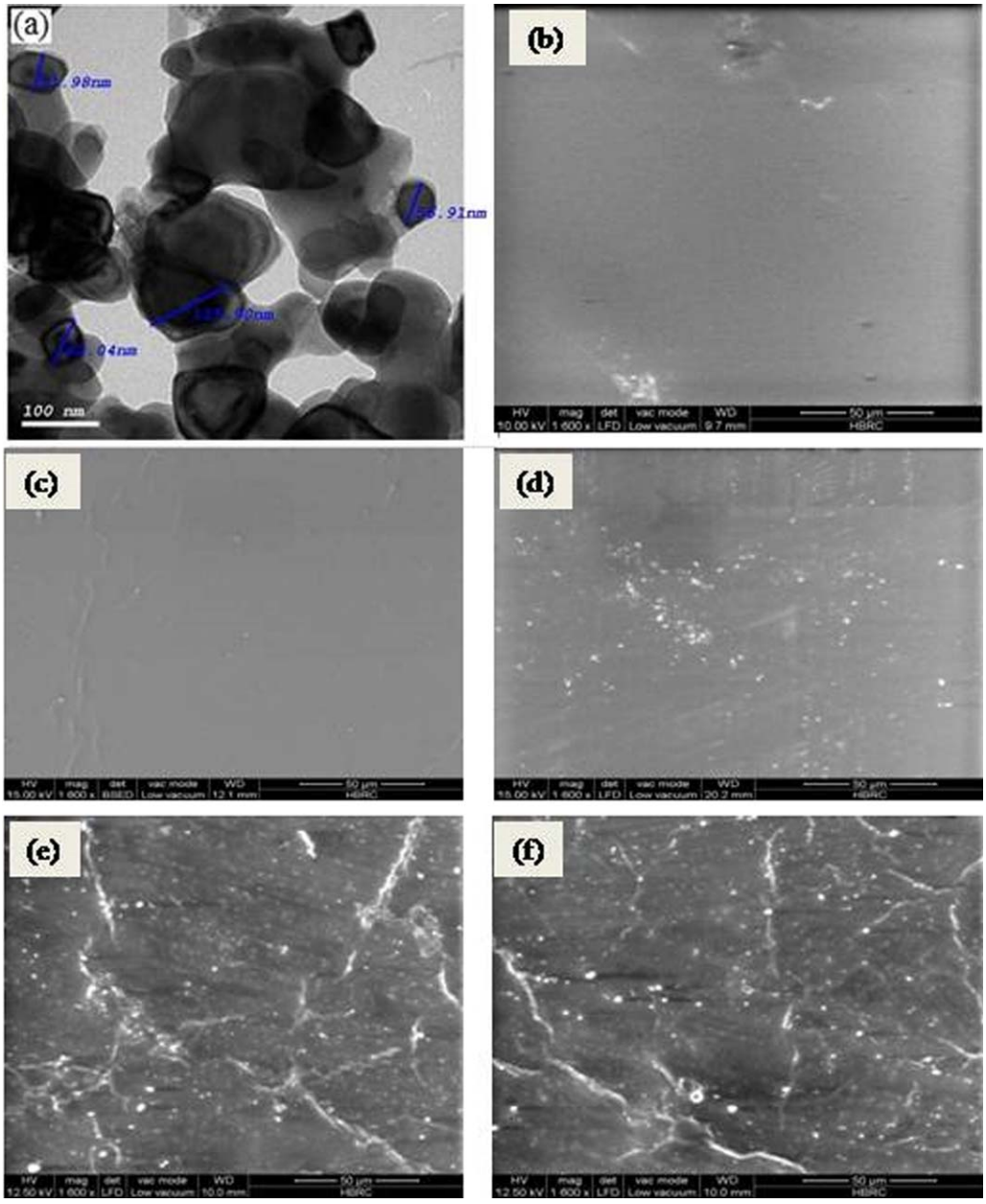

FIG. 2. (a) HR-TEM of CdO nanoparticles and SEM images for: (b) pure PVC, (c) 0.3 wt% CdO-doped PVC, (d) 0.7 wt% CdO-doped PVC, (e) 1.0 wt% CdO-doped PVC, and (f) 1.4 wt% CdO-doped PVC films. [Color figure can be viewed in the online issue, which is available at wileyonlinelibrary.com.]

allowed indirect transitions, respectively [44]. The plot of $(\alpha h\upsilon)^2$ versus $h\upsilon$ at RT enables us to estimate the E_g values by extrapolating the linear part of $(\alpha h\upsilon)^2$ to zero as shown in Fig. 4(a). The obtained E_g values are tabulated in Table 2. For pure PVC, $E_g = 5.08$ eV and it is similar to that reported in Ref. [45]. Also, the values of E_g decreased to 4.88 eV with increasing the CdO content to 1.4 wt%. Such behavior has been reported in different composite polymers [46, 47]. The decrease in E_g values could be attributed to the creation of localized states in the band gap as a result of CdO doping.

The absorption coefficient near the fundamental absorption edge is exponentially dependent on $h\upsilon$ and obeys the empirical Urbach relation. The Urbach energy (E_U) can be calculated by the following relation [48]:

$$\alpha = \alpha_o \exp\left(\frac{h\upsilon - E_I}{E_U}\right) \tag{4}$$

where E_I and α_o are constants. The E_U values were calculated from the slopes of Fig. 4(b), using the relationship: $E_U = (d(ln\alpha)/dh\upsilon)^{-1}$, and the obtained E_U values are given in Table 2. The E_U values of the PVC films are increased with increasing CdO content. One noted that the values of E_U are changed inversely with those of E_g and this may be due to the increase of the disorder of PVC matrix by CdO doping. This increase leads to a

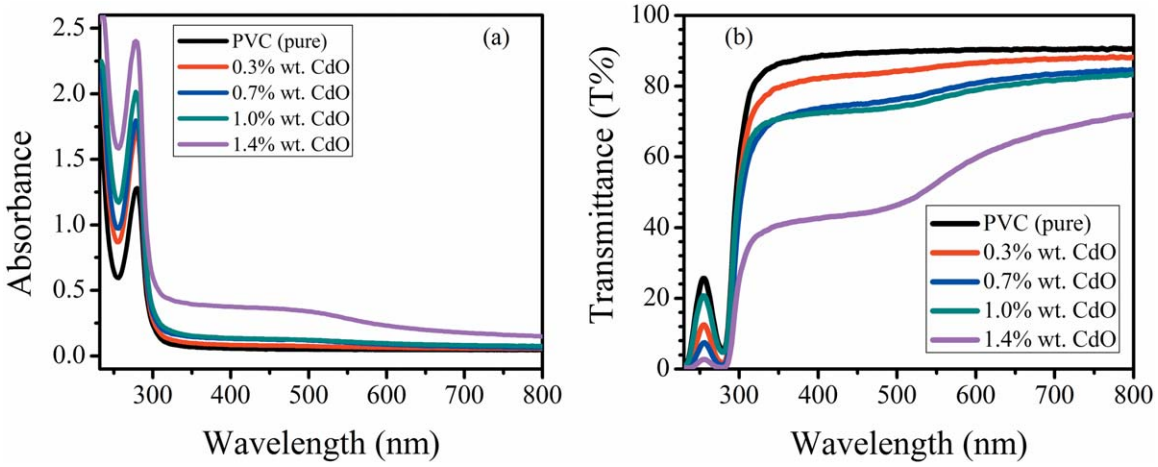

FIG. 3. (a) UV–visible absorption spectra and (b) transmittance spectra of pure PVC and PVC/CdO nanocomposite films. [Color figure can be viewed in the online issue, which is available at wileyonlinelibrary.com.]

redistribution of states from band to tail and thus allows for a large number of possible bands to tail and tail to tail transitions [49].

One of the methods for calculating the refractive index (n) is by using the reflectance (R) and the extinction coefficient, k, (where $k=\alpha\lambda/4\pi$) of films [50]:

$$n=\left(\frac{1+R}{1-R}\right)+\sqrt{\frac{4R}{(1-R)^2}-k^2} \tag{5}$$

where n is the real part of the complex refractive index given by $\tilde{n} = n + ik$, and R is the reflectance that calculated from the absorbance (A) and transmission (T) spectra using the relation; $R=1-\sqrt{(T*\exp(A)}$ [50, 51]. Fig. 5(a) shows the refractive index distributions of pure PVC film and the PVA loaded with CdO nanocparticles. In the visible region, n of pure PVC film is 1.48. Such value has also been measured for PVC with an Abbe's refractometer and a thermostated water circulation system at 30°C by Rajulu et al. [52]. As seen from Fig. 5(a), n of the nanocomposite films are significantly increased with incorporation of the CdO nanoparticles into the PVC matrix similar to PVA/Ag nanocomposites [1]. The changes in the physical properties of a material are strongly dependent on its internal structure, i.e. packing density, molecular weight distributions, etc. The increase in n of PVC after embedding CdO nanoparticles may be due to the formation of intermolecular hydrogen bonding between the oxygen atoms of CdO with the adjacent hydrogen atoms of PVC matrix. Such increase in n may extend the usability of these materials as antireflection coating for solar cells to high refractive index lenses.

From the normal dispersion behavior of n with λ, various dispersion parameters can be calculated on the

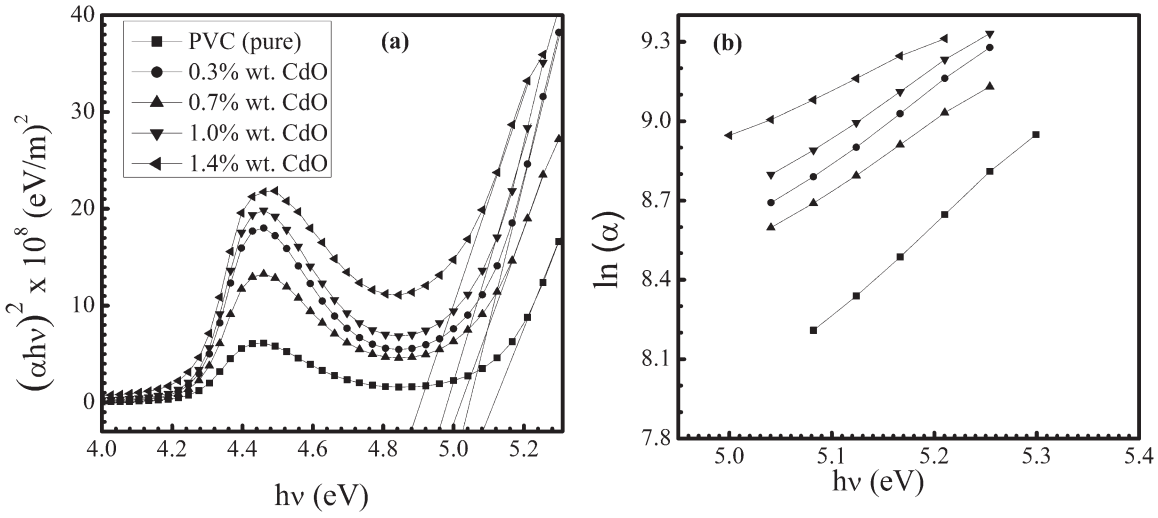

FIG. 4. (a) Plots of $(\alpha h\upsilon)^2$ vs. the photon energy ($h\upsilon$) and (b) $ln\ (\alpha)$ vs. $h\upsilon$ of pure PVC and PVC/CdO nanocomposite films.

 DOI 10.1002/pc

TABLE 2. The direct energy band gap, E_g, Urbach energy, E_U, and various optical dispersion constants for pure PVC and PVA/CdO nanocomposite films.

Sample	E_g (eV)	E_U (eV)	E_d (eV)	E_o (eV)	n_∞	λ_o (nm)	$S_o \times 10^{13}$ (m^{-2})
PVC (pure)	5.08	0.294	5.571	5.68	1.403	213	2.134
0.3%CdO	5.03	0.365	8.135	5.77	1.545	217	2.945
0.7%CdO	5.00	0.391	11.63	5.82	1.720	219	4.083
1.0%CdO	4.96	0.401	14.35	6.28	1.838	142	11.81
1.4%CdO	4.88	0.575	38.78	7.37	2.623	216	12.60

basis of the single oscillator model that developed by DiDomenico and Wemple [53, 54]:

$$n^2 = 1 + \frac{E_d E_o}{E_o^2 - (h\upsilon)^2} \tag{6}$$

where E_d is the energy parameter (a measure of the strength of interband optical transition) and E_o is the single oscillator energy (the average excitation energy for electronic transitions). The values of E_d and E_o can be obtained from the intercept and slope of the linear fitted lines by plotting $(n^2-1)^{-1}$ vs. $(h\upsilon)^2$ as depicted in Fig. 5(b). The obtained values of E_d and E_o are listed in Table 2. Moreover, the variation of the n with λ can be expressed by the relation [55]:

$$\frac{n_\infty^2 - 1}{n^2 - 1} = 1 - \left(\frac{\lambda_o}{\lambda}\right)^2 \tag{7}$$

where n_∞ is the long wavelength refractive index and λ_o is the average interband oscillator wavelength. The parameters n_∞, λ_o, as well as S_o (the average oscillator strength; $S_o = (n_\infty^2 - 1)/\lambda_o^2$) were obtained from the slope and the intercepts of $(n^2-1)^{-1}$ vs. λ^{-2} curves as shown in Fig. 5(c). The values of these parameters are also given in Table 2. It notices that the optical parameters are change with the incorporation of CdO nanoparticles within PVC materix. Therefore, it can suggest that the optical constants of the nanocomposite films could be controlled by CdO content. The quantitative measurements of these parameters may help in tailoring and modeling the properties of such nanocomposites for their use in optical components and devices.

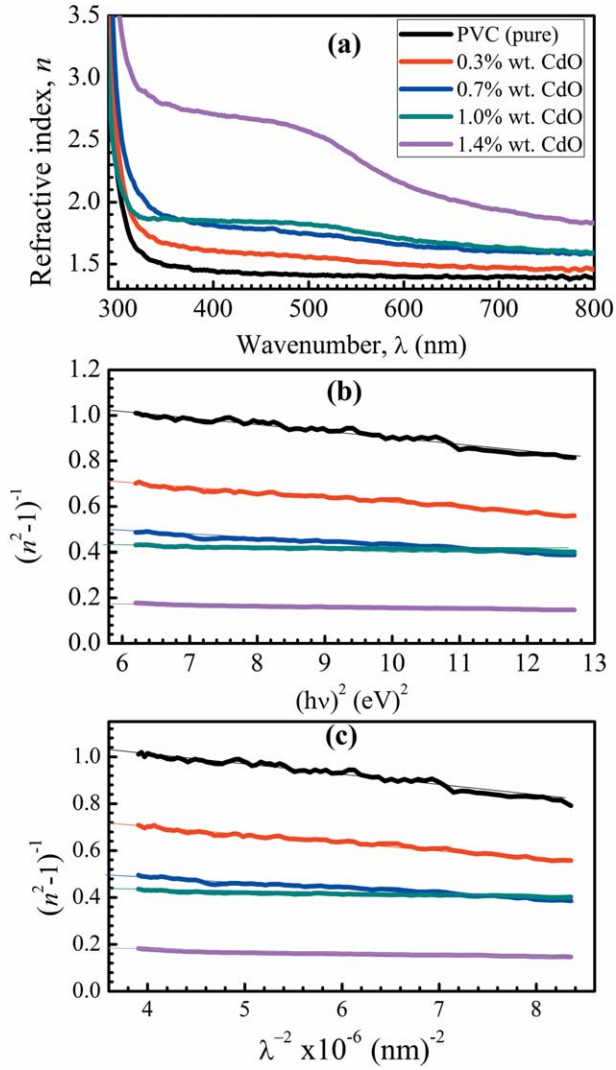

FIG. 5. (a) The dependence of the refractive index (n) on the wavelength (λ), (b) $(n^2-1)^{-1}$ against $(h\upsilon)^2$ plots, and (c) $(n^2-1)^{-1}$ vs. λ^{-2} plots for pure PVC and PVA/CdO nanocomposite films. [Color figure can be viewed in the online issue, which is available at wileyonlinelibrary.com.]

Dielectric Measurements

Dielectric spectroscopy has been proven to be a powerful technique for studying the relaxation and conduction mechanisms in polymeric materials [56]. The dependence of the dielectric constant (ε') on the temperature, T (K) for pure PVC and PVC mixed with CdO nanoparticles at different fixed frequencies is depicted in Fig. 6(a–e). As seen, ε' varies slowly with increasing the temperature up to T_g and then increases with further increase in temperature till reach a saturation region, then it decreases again. There are relaxation peaks, designed α_a, for all PVC samples. This process corresponds to the segmental relaxation associated with the glass transition at which the micro-Brownian motion of long chain segments in the amorphous regions of PVC takes place.

At lower temperatures, the thermal energy that is absorbed by the polymeric material, at a certain fixed frequency, is small and a small number of dipoles can rotate with small angles. The increase of ε' is determined by the number of orienting dipoles per unit volume and their dipole moments [57]. As the temperature is increased, the viscosity of polymeric films is decreased and the dipoles gain sufficient energy and can orient themselves easily in the direction of the applied electric field. Also, the chain segments get sufficient thermal energy to speed up its rotational motion and consequently the increase in

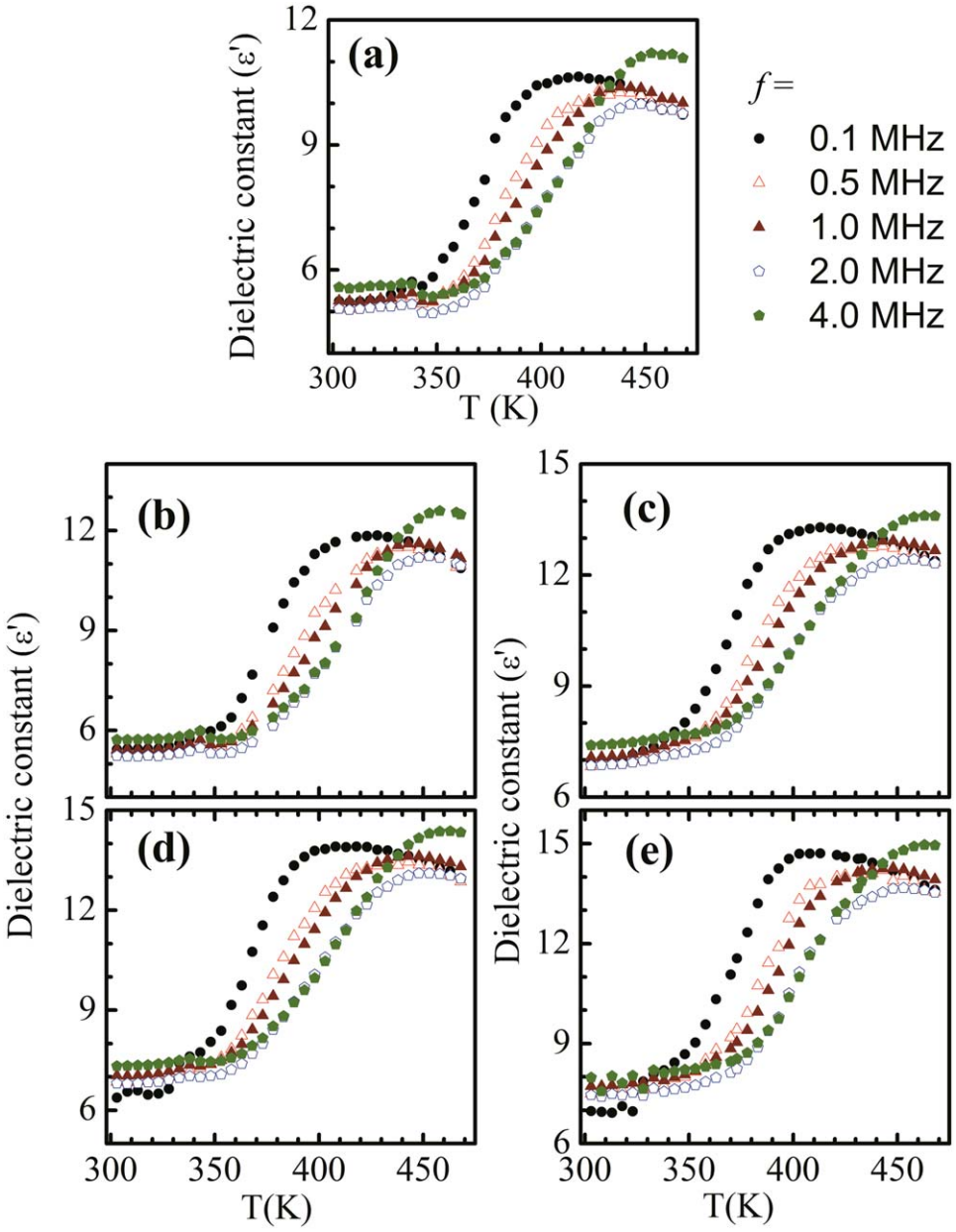

FIG. 6. The variation of the dielectric constant (ε') as a function of temperature and fixed frequency for: (a) Pure PVC, (b) PVC/0.3 wt% CdO, (c) PVC/0.7 wt% CdO, (d) PVC/1.0 wt% CdO and (e) PVC/1.4 wt% CdO. [Color figure can be viewed in the online issue, which is available at wileyonlinelibrary.com.]

polarization occurs [38, 58, 59]. However, the specific volume of the polymer increases with the further increase in temperature, and hence ε' decreases at higher temperatures [60, 61].

It is found that the values of the dielectric constant are less sensitive to the variation of the frequency around RT. In the temperature range 408–468, K the variation in ε' can be indentified than that at 303 K. This means that the increase of temperature has a decisive influence on the dielectric properties of the host material, independently on the degree of CdO nanoparticles incorporation. It is noted that the dielectric constant shifts to higher values after mixing PVC with CdO nanoparticles. There are two main reasons evoked for this increasing in the polarization with increasing CdO nanoparticles content; first the interfacial polarization results from the heterogeneous structure of nanocomposites, facilitating the formation of CdO network within PVC matrix. Second is due to the intrinsic ionic polarization of PVC matrix.

To give more evidence for the reinforcement of the dielectric permittivity of pure PVC with filling with CdO nanoparticles, the variation of ε' with field frequency at various temperatures for all studied nanocomposite films

 DOI 10.1002/pc

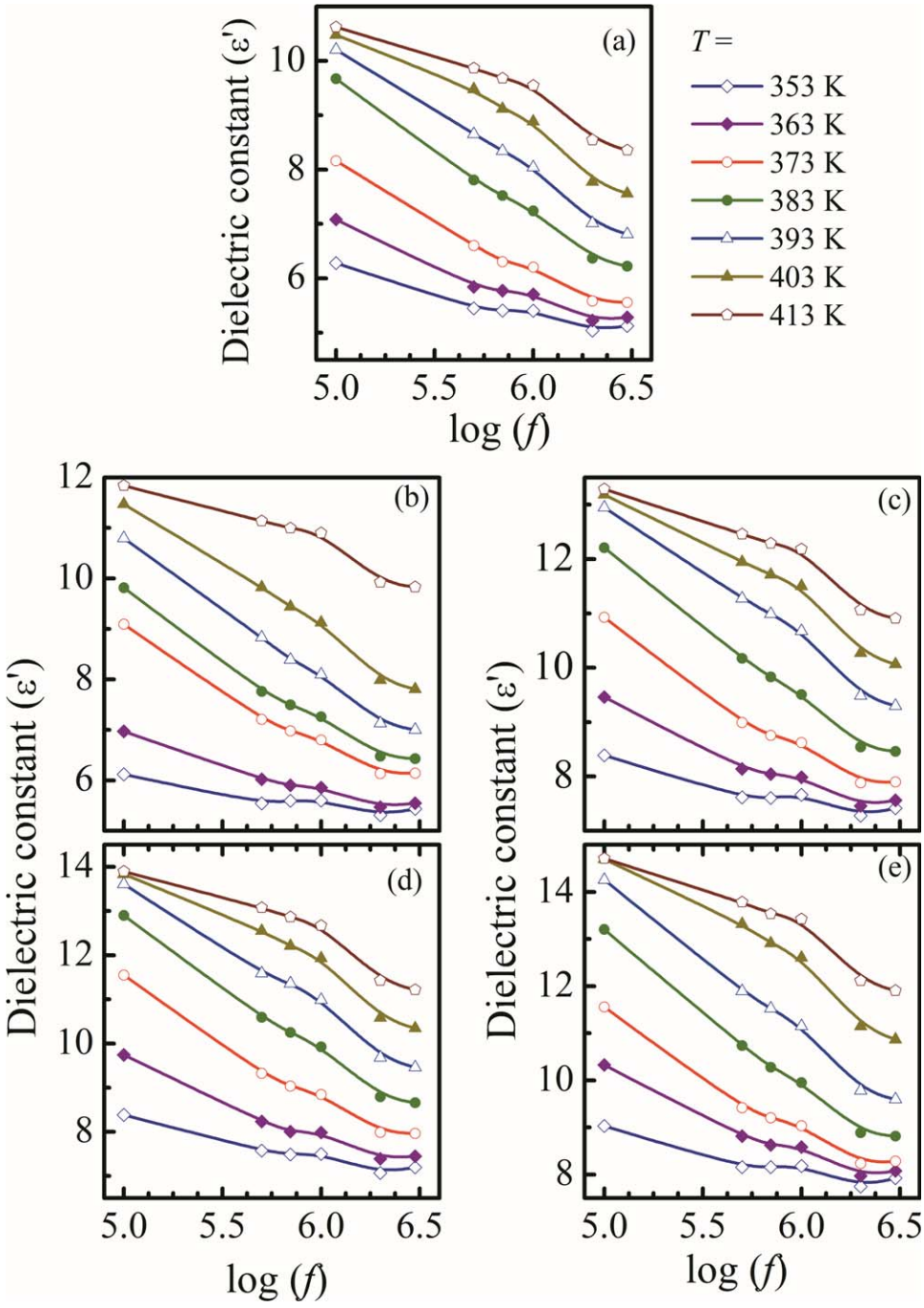

FIG. 7. The frequency dependence of the dielectric constant (ε') at various temperatures for: (a) pure PVC, (b) PVC/0.3 wt% CdO, (c) PVC/0.7 wt% CdO, (d) PVC/1.0 wt% CdO and (e) PVC/1.4 wt% CdO. [Color figure can be viewed in the online issue, which is available at wileyonlinelibrary.com.]

is displayed in Fig. 7(a–e). As seen, ε' decreases with increasing the field frequency due to decreasing of the number of dipoles which contribute to polarization. In addition, ε' of pure PVC increases with increasing the content of CdO nanoparticles in the PVC matrix.

To investigate the influence of adding the CdO nanoparticles on the ac conductivity (σ_{ac}) of PVC films, the σ_{ac} values were calculated using the relation;

$$\sigma_{ac} = \omega \varepsilon_o \varepsilon' \tan\delta = 2\pi f \varepsilon_o \varepsilon'' \quad (8)$$

where ω is the angular frequency ($\omega = 2\pi f$), f is the applied frequency, ε_o is the permittivity of the free space, $\tan\delta = \varepsilon''/\varepsilon'$ and ε'' represents the dielectric loss. Fig. 8(a–e) represents the measured ac conductivity ($log\ \sigma_{ac}$) as a function of the reciprocal of temperature ($1000/T$) for the PVC and PVC loaded with CdO nanoparticles. It is clear that σ_{ac} of each

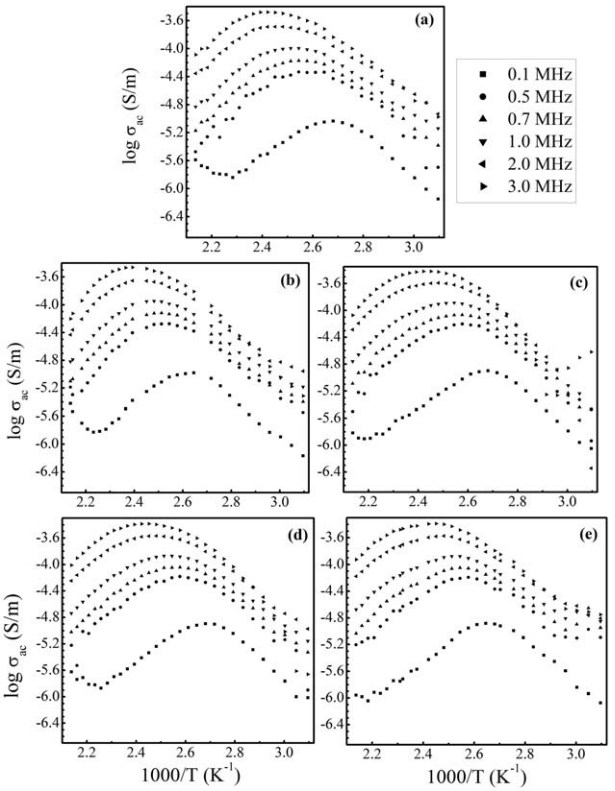

FIG. 8. The variation of log (σ_{ac}) versus 1000/T for: (a) Pure PVC, (b) PVC/0.3 wt% CdO, (c) PVC/0.7 wt% CdO, (d) PVC/1.0 wt% CdO and (e) PVC/1.4 wt% CdO.

sample increases with increasing the applied frequency. The overall temperature dependent conductivity curves can be separated into two distinct regions. At low temperatures, the conductivity is enhanced. This may be due to either the available thermal activation of the polymer chains or the phase transition of the polymer system from semi-crystalline to amorphous. The peaks of the curves are shifted to higher temperatures with increasing f. A retreating in the conductivity with rising temperature is occurring. Similar trends in the conductivity-temperature dependent, has been reported in Ref. [62].

The highest values of σ_{ac} for all investigated samples at $f = 0.1$ and 3 MHz and their corresponding temperature are summarized in Table 3. For pure PVC, σ_{ac} is in the order of 10^{-5} S/m which is consistent with the measured value by Goyal et al. [63]. On the other hand, the values of σ_{ac} for PVC are increased with increasing the content of CdO nanoparticles. The homogenous distribution of CdO nanoparticle, which confirmed from SEM images (Fig. 2(c–f)), allows the formation of more numbers of conductive three-dimensional networks throughout the nanocomposite and assists the charge carriers to hop from conducting clusters to neighbors. These observations agreed with the published data for different polymers and amorphous semiconductors [16, 64, 65]. Furthermore, the increase of σ_{ac} and the decrease of E_g with increasing CdO content inside PVC reveal that both the optical and dielectric measurements are in agreement with each other.

TABLE 3. The highest values of ac conductivity at frequencies, $f = 0.1$ and 3 MHz for pure PVC and PVC/CdO films.

	$\sigma_{ac} \times 10^{-5}$ (S/m) at different f	
Sample	0.1 MHz	3 MHz
PVC	0.92 (at 373 K)	33.18 (at 413 K)
0.3% wt CdO	1.04 (at 383 K)	34.52 (at 418 K)
0.7% wt CdO	1.26 (at 373 K)	38.18 (at 413 K)
1.0% wt CdO	1.27 (at 373 K)	41.13 (at 408 K)
1.4% wt CdO	1.31 (at 378 K)	40.77 (at 408 K)

CONCLUSIONS

It has been demonstrated that adding the sol-gel synthesized CdO nanoparticles into the PVC films has analysis induces significant modifications in both the optical and dielectric properties. XRD analysis indicated that the crystal structure of the CdO is cubic with Fm3m space symmetry group while PVC has a typical semi-crystalline nature. The direct optical energy band gap (E_g) showed a red-shift from 5.08 to 4.88 eV. The refractive index of the pure PVC is 1.48 and increased significantly with increasing the CdO content and the optical dispersion constants were also changed. The dielectric constant increased with the addition of CdO nanoparticles to PVC due to the interfacial polarization. Also, the ac conductivity increased with increasing CdO content. These results may reflect the importance applications of these nanocomposite films such as optical and/or electrical devices.

REFERENCES

1. R.P. Chahal, S. Mahendia, A.K. Tomar, and S. Kumar, *J. Alloys Compd.,* **538**, 212 (2012).
2. W. Wu, S. Liang, L. Shen, Z. Ding, H. Zheng, W. Su, and L. Wu, *J. Alloys Compd.,* **520**, 213 (2012).
3. Y. Zare, *Waste Manage*. **33**, 598 (2013).
4. S. Cho and W. Choi, *J. Photochem. Photobiol. A: Chem.,* **143**, 221 (2001).
5. L. Fang, Y.-H. Song, X.-N. Zheng, S.-H. Chen, P.-H. Da, and Q. Zheng, *Chin. J. Polym. Sci.,* **28**, 637 (2010).
6. H. Yoo and S.-Yeop Kwak, *Appl. Catal. B Environ.,* **104**, 193 (2011).
7. F. Liu, H. Liu, X. Li, H. Zhao, D. Zhu, Y. Zheng, and C. Li, *Appl. Surf. Sci.,* **258**, 4667 (2012).
8. N. Reddeppa, A.K. Sharma, V.V.R.N. Rao, and W. Chen, *Microelectron. Eng.,* **112**, 57 (2013).
9. Y.-X. Zhang, Y.-H. Song, and Q. Zheng, *Chin. J. Polym. Sci.,* **31**, 325 (2013).
10. A. Olad, S. Behboudi, and A.A. Entezami, *Chin. J. Polym. Sci.*, **31**, 481 (2013).

 DOI 10.1002/pc

11. O.A. Al-Hartomy, F. Al-Salamy, A.A. Al-Ghamdi, M. Abdel Fatah, N. Dishovsky, and F. El-Tantawy, *J. Appl. Polym. Sci*., **120**, 3628 (2011).
12. A.A. Al-Ghamdi, F. El-Tantawy, N. Abdel Aal, E.H. El-Mossalamy, and W.E. Mahmoud, *Polym. Degrad. Stab*., **94**, 980 (2009).
13. W.E. Mahmoud and A.A. Al-Ghamdi, *Polym. Compos*., **32**, 1143 (2011).
14. I.S. El ashmawi, N.A. Hakeem, L.K. Marei, and F.F. Hanna, *Phys. B*, **405**, 4163 (2010).
15. A. Olad and R. Nosrati, *Prog. Organ. Coat*., **76**, 113 (2013).
16. F. Ma, N. Yuan, and J. Ding, *J. Appl. Polym. Sci*., **128**, 3870 (2013).
17. I. Kemal, A. Whittle, R. Burford, T. Vodenitcharova, and M. Hoffman, *J. Appl. Polym. Sci*., **127**, 2339 (2012).
18. T. Sterzynski, J. Tomaszewska, K. Piszczek, and K. Skórczewska, *Compos. Sci. Technol*., **70**, 966 (2010).
19. C.C. Vidyasagar, Y.A. Naik, T.G. Venkatesh, and R. Viswanatha, *Powder Technol*., **214**, 337 (2011).
20. H. Colak and O. Turkoglu, *Mater. Sci. Semicond. Process*., **16**, 712 (2013).
21. F. Yakuphanoglu, *Sol. Energy*, **85**, 2704 (2011).
22. S. Calnan and A.N. Tiwari, *Thin Solid Films*, **518**, 1839 (2010).
23. C.J. Ksanda, *Am. J. Sci*., **22**, 131 (1931).
24. A.M. Bazargan, S.M.A. Fateminia, M.E. Ganji, and M.A. Bahrevar, *Chem. Eng. J*., **155**, 523 (2009).
25. M.A. F.-Mendoza, R. C.-Perez, G. T.-Delgado, S.A. Tomas, J.G. M.-Alvarez, and O. Z.-Angel, *J. Lumin*., **130**, 2500 (2010).
26. A. Tadjarodi, M. Imani, and H. Kerdari, *Mater. Res. Bull*., **48**, 935 (2013).
27. A. Tadjarodi and M. Imani, *Mater. Lett*., **65**, 1025 (2011).
28. M. Benhaliliba, C.E. Benouis, A. T.-Silver, F. Yakuphanoglu, A. A.- Garcia, A. Tavira, R.R. Trujillo, and Z. Mouffak, *J. Lumin*., **132**, 2653 (2012).
29. S. Reddy, B.E.K. Swamy, U. Chandra, B.S. Sherigara, and H. Jayadevappa, *Int. J. Electrochem. Sci*., **5**, 10 (2010).
30. J.K. Andeani and S. Mohsenzadeh, Journal of Chemistry, 2013, Article ID 147613, 4 (2013). http://dx.doi.org/10.1155/2013/147613.
31. S. Kondawar, R. Mahore, A. Dahegaonkar, and S. Agrawal, *Adv. Appl. Sci. Res*., **2**, 401 (2011).
32. A.S. Roy, K.P. Anilkumar, and M. V. N.A. Prasad, *J. Appl. Polym. Sci*., **123**, 1928 (2012).
33. W.E. Mahmoud, M. Hafez, N.A. El-Aal, and F. El-Tantawy, *Polym. Int*., **57**, 35 (2008).
34. W.E. Mahmoud, *Eur. Polym. J*., **47**, 1534 (2011).
35. N.S. Allen, M. Edge, M. Rodriguez, C.M. Liauw, and E. Fontan, *Polym. Degrad. Stab*., **68**, 363 (2000).
36. S. Giuffrida, G.G. Condorelli, L.L. Costanzo, G. Ventimiglia, A.D. Mauro, and I.L. Fragal, *J. Photochem. Photobiol. A: Chem*., **195**, 215 (2008).
37. S.H. Mortazavi, M. Ghoranneviss, and S. Faryadras, *J. Fusion Energ*., **31**, 211 (2012).
38. A. Hassen, A.M. El Sayed, W.M. Morsi, and S. El-Sayed, *J. Appl. Phys*., **112**, 093525 (2012).
39. M. S. Augustine, P.P. Jeeju, V. G. Sreevalsa, and S. Jayalekshmi, *J. Phys. Chem. Solids*, **73**, 396 (2012).
40. W.E. Mahmoud, A.A. Al-Ghamdi, and F. Al-Agel, *Polym. Advan. Technol*., **22**, 2055 (2011).
41. W.E. Mahmoud, W. Shirbeeny, A.A. Al-Ghamdi, and S. Al-Heniti, *J. Appl. Polym. Sci*., **125**, 339 (2012).
42. M. Dutta, S. Mridha, and D. Basak, *Appl. Surf. Sci*., **254**, 2743 (2008).
43. E.F. Keskenler, G. Turgut, and S. Dogan, *Superlatt. Microstruc*., **52**, 107 (2012).
44. R. Wen, L. Wang, X. Wang, G.H. Yue, Y. Chen, and D.L. Peng, *J. Alloys Compd*., **508**, 370 (2010).
45. A. Ahmed, T. Najim, J. Salimon, N. Salih, A. Graisa, Y. Farina, and E. Yousif, *ARPN J. Eng. Appl. Sci*., **5**, 43 (2010).
46. K.R. Mohan, V.B.S. Achari, V.V.R.N. Rao, and A.K. Sharma, *Polym. Test*., **30**, 881 (2011).
47. P.C. Sekhar, P.N. Kumar, U. Sasikala, V.V.R.N. Rao, and A.K. Sharma, *Eng. Sci. Technol.: Int. J*., **2**, 908 (2012).
48. F. Urbach, *Phys. Rev*., **92**, 1324 (1953).
49. S.K. O'Leary, S. Zukotynski, and J.M. Perz, *J. Non-Cryst. Solids*, **210**, 249 (1997).
50. I.S. Yahia, A.A.M. Farag, M. Cavas, and F. Yakuphanoglu, *Superlattices Microstruct*., **53**, 63 (2013).
51. A.M. El Sayed, and W.M. Morsi, *Polym. Compos*., **34**, 2031 (2013).
52. A.V. Rajulu, R.L. Reddy, S.M. Raghavendra, and S.A. Ahmed, *Eur. Polym. J*., **35**, 1183 (1999).
53. W. Sellmeier, *Ann. Phys. Chem*., **143**, 271 (1871).
54. S.H. Wemple, and M. DiDomenico, *Phys. Rev. B*, **3**, 1338 (1970).
55. B.J. Zheng, J.S. Lian, L. Zhao, and Q. Jiang, *Appl. Surf. Sci*., **253**, 2910 (2010).
56. A. Karmakar, and A. Ghosh, *J. Appl. Phys*., **110**, 134101 (2011).
57. S. Mahrous, *Polym. Int*., **40**, 261 (1996).
58. A. Belal, M. Amin, H. Hassan, A. Abd El-Mongy, B. Kamal, and K. Ibrahim, *Phys. Status Solidi A*, **144**, k53 (1994).
59. T.A. Hanafy, *J. Appl. Polym. Sci*., **108**, 2540 (2008).
60. Ch.V.S. Reddy, X. Han, Quan.-Y. Zhu, Li.-Q. Mai, and W. Chen, *Microelectron. Eng*., **83**, 281 (2006).
61. V. Rao, P.V. Ashokan, and M.H. Shridhar, *Mater. Sci. Eng*., **A281**, 213 (2000).
62. A.A. Mohamad, and A.K. Arof, *Ionics*, **12**, 263 (2006).
63. M.G. Kulthe, and R.K. Goyal, *Adv. Mater. Lett*., **3**, 246 (2012).
64. M.D. Migahed, M. Ishra, T. Fahmy, and A. Barakat, *J. Phys. Chem. Solids*, **65**, 121 (2004).
65. S.A. Saqan, A.S. Ayesh, A. M. Zihlif, E. Martuscelli, and G. Ragosta, *Polym. Test*., **23**, 739 (2004).